Switching between coexisting stable periodic solutions by impulsive forces with an application to a vibrating plate

D.W.M. Veldman*, R.H.B. Fey*, and H.J. Zwart *,**
*Dept. of Mechanical Engineering, Eindhoven University of Technology, Eindhoven, the Netherlands
**Dept. of Applied Mathematics, University of Twente, Enschede, the Netherlands

Summary. Single-degree-of-freedom nonlinear mechanical systems under periodic excitation may possess coexisting stable periodic solutions. Depending on the application, one of these stable periodic solutions is desired. We propose two algorithms to design an impulsive force that will bring the system from an undesired to a desired stable periodic solution. Both algorithms have a variant that requires only limited information about the applied force. We illustrate our method for a single-degree-of-freedom model of a rectangular plate with geometric nonlinearity, which takes the form of a monostable forced Duffing equation with hardening nonlinearity.

Introduction

We consider a controlled single-degree-of-freedom (single-DOF) mechanical system with periodic excitation,

$$\dot{x}_1(t) = x_2(t), \qquad m\dot{x}_2(t) = F(\mathbf{x}(t)) + F_e(t) + F_c(t). \tag{1}$$

The state-vector $\mathbf{x}(t) = [x_1(t), x_2(t)]^\top$ has a position component $x_1(t)$ and a velocity component $x_2(t)$. The coefficient $m > 0$ represents the (effective) mass, $F(\mathbf{x}(t))$ represents the internal forces acting on the mass, $F_e(t) = F_e(t+T)$ is the periodic excitation with $T > 0$ the period of $F_e(t)$, and $F_c(t)$ is the open loop control force. We assume that the system (1) shows coexisting stable periodic solutions in the absence of the control force $F_c(t)$.
In this paper, we propose two practical algorithms to design an impulsive force $F_c(t)$ which guarantees a switch from an undesired to a desired periodic solution. Alternative approaches can be found in [1, 2]. The proposed algorithms may be applied in energy harvesting, in which nonlinear resonators are used to widen the bandwidth in which significant power can be harvested. For this application, switching to a large-amplitude periodic solution may improve performance. The algorithms may also be applied in vibration reduction problems, for a switch to a small-amplitude periodic solution.

Control algorithms

First, we study the situation where the control force $F_c(t)$ is a Dirac delta. Consider the situation in Fig. 1, which shows two stable periodic solutions (• dots) and one unstable periodic solution (◦ dot) of (1) in the Poincaré section at $t = t_0$. The stable manifold of the unstable periodic solution separates the domains of attraction of the desired and undesired periodic solution (white and grey areas, resp.). The arrow indicates the change in velocity due to a Dirac delta in the control force, i.e. $F_c(t) = G_c\delta(t - t_0)$ with G_c the linear impulse of the control force. Note that the resulting change in velocity G_c/m moves the solution from the undesired to the desired domain of attraction, see Fig. 1.
A real actuator can not realize a true Dirac-delta impulsive force. Therefore, the pulse is assumed to be applied during a short time interval $[t_0, t_0 + \Delta t]$. We have two algorithms for selecting the linear impulse G_c and triggering time t_0 of the control force. Later, we will discuss how to choose the maximally allowed pulse duration Δt. Intuitively, it is clear that the exact 'shape' of the impulsive force is not important when Δt is small. In both algorithms, we select a solution $\mathbf{y}(t) = [y_1(t), y_2(t)]^\top$ in the (white) desired domain of attraction. In Algorithm 1, we choose t_0 as the moment at which the current state $\mathbf{x}(t)$ (in the undesired domain of attraction) and $\mathbf{y}(t)$ have the same position coordinate, i.e. $x_1(t_0) = y_1(t_0)$, and determine G_c from the velocity difference at that time, i.e. $G_c = m(y_2(t_0) - x_2(t_0))$. In Algorithm 2, we determine G_c and t_0 by aiming at the error $\mathbf{e}(t) := \mathbf{x}(t) - \mathbf{y}(t)$ to be zero at the end of the pulse (i.e. $\mathbf{e}(t_0 + \Delta t) = \mathbf{0}$).

Single-DOF plate model with geometric nonlinearity

We illustrate the algorithms for a single-DOF model of a rectangular plate. The edges of the plate are clamped and have a harmonic acceleration in the out-of-plane direction $\ddot{w}_e(t) = \bar{w}_e \cos(2\pi f_e t)$. The large-amplitude vibrations of plates are described by the Föppl-Von Karman equations. In a Cartesian coordinate system (x, y, z), these equations are formulated

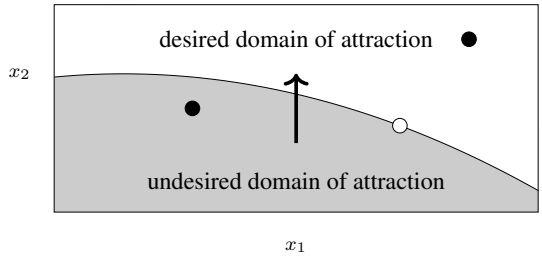

Figure 1: Domains of attraction in the Poincaré section

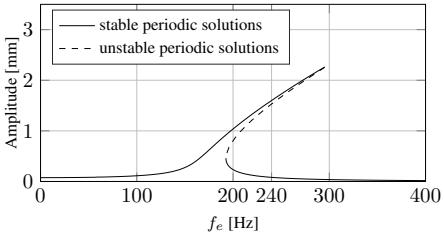

Figure 2: Amplitude-frequency diagram

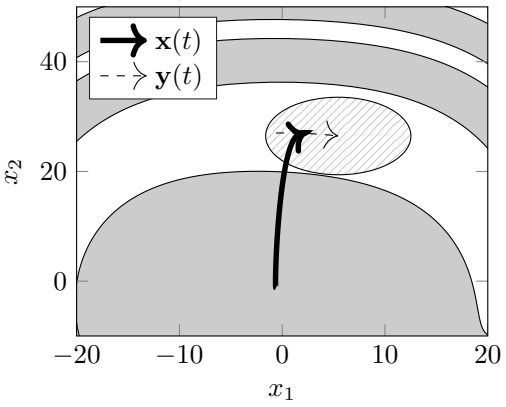

Figure 3: Application of Algorithm 1 ($\Delta t = 0.05T$)

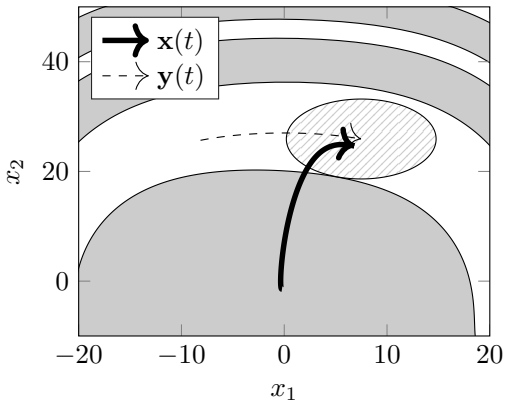

Figure 4: Application of Algorithm 2 ($\Delta t = 0.13T$)

in terms of the out-of-plane displacement field $w(x, y, t)$, and two in-plane displacement fields. We use a single-mode approximation $w(x, y, t) = q(t)W(x, y)$, where $q(t)$ is the generalized coordinate and $W(x, y)$ approximates the lowest out-of-plane eigenmode. The in-plane displacement fields can be expressed in terms of $q(t)$ by solving the quasi-static in-plane equations (neglecting in-plane inertia). This results in a monostable Duffing equation with a hardening nonlinearity. For a $300 \times 200 \times 1$ mm^3 aluminum plate with $\bar{w}_e = 50$ m/s^2, we find the amplitude-frequency plot in Fig. 2 (amplitude = $(\max(q) - \min(q))/2$). At $f_e = 240$ Hz, we write the equation for $q(t)$ to its dimensionless form and find

$$\dot{x}_1(t) = x_2(t), \qquad \dot{x}_2(t) = -2\zeta x_2(t) - x_1(t) - \mu x_1^3(t) + \cos(\omega t) + F_c(t), \tag{2}$$

with $\zeta = 0.01$, $\mu = 0.003$, and $\omega = 1.3906$. Note that (2) is of the form (1).
Figs. 3 and 4 show Poincaré sections at $t = t_0 + \Delta t$, with the desired (in white) and undesired (in grey) domains of attraction. The arrows, however, indicate the trajectories of $\mathbf{x}(t)$ and $\mathbf{y}(t)$ for $t \in [t_0, t_0 + \Delta t]$ resulting from Algorithm 1 (Fig. 3) and Algorithm 2 (Fig. 4) from the section "Control algorithms". The hatched elliptic disks lying in the desired domain of attraction will be discussed below.

Determining the maximally allowed pulse duration Δt

In the section "Control algorithms", we introduced two algorithms to determine the triggering time t_0 and the linear impulse of the control force G_c. We now discuss how to choose Δt. A maximally allowed pulse duration Δt can be determined for both algorithms using Figs. 3 and 4: the hatched elliptic disks in these figures are centered at $\mathbf{y}(t_0 + \Delta t)$ and are guaranteed to contain $\mathbf{x}(t_0 + \Delta t)$. Thus, when the hatched elliptic disk is completely contained in the (white) desired domain of attraction, the applied impulsive force will result in the desired steady-state behavior. The maximally allowed pulse duration is found when the hatched elliptic disk touches the border of the desired domain of attraction. The shape of the pulse was used to construct the elliptic disks in Fig. 3 (where $\Delta t = 0.05T$) and Fig. 4 (where $\Delta t = 0.13T$). If we only use the information that the linear impulse of $F_c(t)$ is G_c and that $F_c(t)$ does not change sign, we find smaller allowed pulse durations: $\Delta t = 0.027T$ for Algorithm 1 and $\Delta t = 0.065T$ for Algorithm 2.
The elliptic disks are constructed based on an 'expected' trajectory $\mathbf{C}(t) = [C_1(t), C_2(t)]^\top$ for the error $\mathbf{e}(t) := \mathbf{x}(t) - \mathbf{y}(t)$. The expected trajectory $\mathbf{C}(t)$ is based on the assumption that $F_c(t)$ will be dominant over $F(\mathbf{x}(t))$ and $F_e(t)$ in (1) for $t \in [t_0, t_0 + \Delta t]$, so that $F(\mathbf{x}(t))$ and $F_e(t)$ can be neglected. We then consider the error introduced by this assumption $\mathbf{z}(t) = [z_1(t), z_2(t)]^\top := \mathbf{e}(t) - \mathbf{C}(t)$. A natural measure for the magnitude of $\mathbf{z}(t)$ is the Lyapunov function $Z(t) := mz_2^2(t) + kz_1^2(t)$. After finding the dynamics of $Z(t)$, we are able to find a bound on $Z(t_0 + \Delta t)$ by the Bihari-Lasalle Lemma. This bound gives then the size of the elliptic disk. Details can be found in [3].
Finally, we note that in the implementation of the algorithms an error may be introduced. For example, in Algorithm 1 (introduced at the end of section "Control algorithms") it might not hold that $x_1(t_0) = y_1(t_0)$ at the moment $t = t_0$ at which the impulsive force is applied, and a slight error $\varepsilon_1 = y_1(t_0) - x_1(t_0)$ is made. These type of implementation errors can be incorporated in the construction of the elliptic disks.

Conclusions

We have proposed two algorithms to design an impulsive force to switch from an undesired to a desired periodic solution and demonstrated them for a single-DOF model of a rectangular plate with geometric nonlinearity.

References

[1] Nijmeijer H., Berghuis H. (1995), On Lyapunov control of the Duffing equation, *IEEE Trans. Circuits Syst. I, Fundam. Theory Appl.* **42**(8), 473-477.

[2] Liu Y., Wiercigroch M., Ing J., Pavlovskaia E. (2013), Intermittent control of coexisting attractors, *Phil. Trans. R. Soc. A* **371**, 20120428.

[3] Veldman D., Fey R., Zwart H. (2017), Impulsive Steering Between Coexisting Stable Periodic Solutions With an Application to Vibrating Plates, *ASME. J. Comput. Nonlinear Dynam.* **12**(1), 011013.